Impedance Control of Hydraulic Series Elastic Actuator with a Model-Based Control Design

Pauli Mustalahti and Jouni Mattila

Abstract— **Traditional mechanical actuators are designed with a high stiffness, which increases the system bandwidth. The operation of stiff actuator in uncertain environments is a challenging task due to physical interactions with the environment. Series elastic actuators (SEAs) have become the prominent method for decreasing stiffness between power output shafts and the environment in electric torque-controlled light arm applications. Compared to lightweight arms, the hydraulic actuated SEAs (HSEAs) can provide a much higher power-to-weight ratio. However, the control design for an HSEA is a challenging task due to the high non-linear dynamics of hydraulic systems. In this study, a novel subsystem-dynamics-based controller for an HSEA is designed using the virtual decomposition control (VDC) approach as a framework. The designed controller is incorporated as an inner-loop controller for previously designed a novel impedance controller. The one degrees-of-freedom (DOF) experimental setup is used to verify the control performance of the proposed controller.**

I. Introduction

In the future, the collaboration of humans and robots will become common in workplaces, homes, and service environments as the field of robotics rapidly advances. Human-robot collaboration requires safe, smooth control, and high-performing robots. One major challenge for the stable position control design is that in uncertain environments, the controller can be affected by unpredictable physical interactions with the environment. Therefore, force control is needed to handle environment dynamics in a closed-loop control.

Series elastic actuators (SEAs) have become a fundamental method in torque-controlled lightweight arm (LWA) in electric applications [1]–[4]. SEAs use a mechanical spring to decouple power output shafts from the environment. This provides force sensing, impact tolerance, and force fidelity for the mechanical actuator. SEAs have been used in different robot applications such as electric humanoid robots [5], [6] and walking robots [7]. Electric SEAs provide a rapid movement with a light load mass and actuator output power. Compared to electric SEAs, the HSEA systems provide a higher power-to-weight ratio and a lower speed ratio. The HSEA for light-duty manipulation is presented in [8], [9]. As presented in [8], the major challenges of the HSEAs in LWA are lack of back-driveability and a low maximum speed. Furthermore, creating a high performance control design for the HSEA systems is a challenging task due to significant nonlinearities of the hydraulic dynamics.

Impedance control for torque-controlled LWA is still an active research topic [10]–[14]. In [10], [14], the disturbance observer based impedance control is presented. In [11] the cascade control is used to decouple the slow outer-loop controller from the fast inner-loop dynamics. The control stability with different environments has been studied [12]. Control design for a linear electric actuator is presented in [15], where high motor voltage with drivetrain is used to produce continuous actuator force. In [16], the position-based impedance controller for the hydraulic drive unit of a legged robot is presented. The most of proposed impedance control methods are verified with torque-controlled LWA.

In this study, we investigated to study control for the HSEA targeted to heavy-duty applications with the payload of 200 kilos. As reported in [17], the nonlinear model-based control methods can provide high control performance with hydraulic manipulators. In previous studies [18]–[20], virtual decomposition control (VDC) shown to lead to state-of-the-art control performance with heavy-duty hydraulic manipulators. In this study, the main focus is to design model-based controller for the HSEA by exploiting the control design a principles of the VDC approach. The proposed controller is incorporated with a novel impedance controller [19].

The paper is organized as follows. First, in Section II the foundation of the VDC approach are presented. The kinematics and dynamics modeling of the HSEA in a view of VDC approach are presented in Section III. The corresponding control equations for the studied system are defined in Section IV. In Section V, the impedance controller for the HSEA is given. Finally, the experimental results are presented in a Section VI, and conclusions are given in Section VII.

II. Mathematical Foundation

In this section, the necessary mathematical foundations of the VDC approach are introduced. Assume that there is an orthogonal three-dimensional coordinate frame $\{\mathbf{A}\}$ attached to the rigid body. Then, it follows from [21] that the linear/angular velocity vector in coordinate frame $\{\mathbf{A}\}$ can be defined as ${}^{\mathbf{A}}V = [{}^{\mathbf{A}}\mathbf{v} \;\; {}^{\mathbf{A}}\boldsymbol{\omega}]^T$. In vector ${}^{\mathbf{A}}V$, ${}^{\mathbf{A}}\mathbf{v} \in \mathbb{R}^3$ denotes the linear velocity vector, and ${}^{\mathbf{A}}\boldsymbol{\omega} \in \mathbb{R}^3$ denotes the angular velocity vector. Furthermore, the force/moment vector, in coordinate frame $\{\mathbf{A}\}$ can be written as ${}^{\mathbf{A}}F = [{}^{\mathbf{A}}\mathbf{f} \;\; {}^{\mathbf{A}}\mathbf{m}]^T$. In this vector, ${}^{\mathbf{A}}\mathbf{f} \in \mathbb{R}^3$ denotes the force vector and ${}^{\mathbf{A}}\mathbf{m} \in \mathbb{R}^3$ denotes the moment vector. For the two fixed successive frames $\{\mathbf{A}\}$ and $\{\mathbf{B}\}$, the following restrictions hold:

$$ {}^{\mathbf{B}}V = {}^{\mathbf{A}}\mathbf{U}_{\mathbf{B}}^{T}\,{}^{\mathbf{A}}V \tag{1} $$

$$ {}^{\mathbf{A}}F = {}^{\mathbf{A}}\mathbf{U}_{\mathbf{B}}\,{}^{\mathbf{B}}F, \tag{2} $$

where ${}^{\mathbf{A}}\mathbf{U}_{\mathbf{B}} \in \mathbb{R}^{6\times 6}$ denotes the force/moment transformation between two fixed coordinate frames.

Pauli Mustalahti and Jouni Mattila are with the Faculty of Engineering and Natural Sciences, Tampere University, Tampere, Finland. Emails: {pauli.mustalahti, jouni.mattila}@tuni.fi

In view of [21], the dynamics in coordinate frame $\{\mathbf{A}\}$ can be expressed as

$$ {}^{\mathbf{A}}F^{*} = \mathbf{M}_{\mathbf{A}}\frac{d}{dt}({}^{\mathbf{A}}V) + \mathbf{C}_{\mathbf{A}}({}^{\mathbf{A}}\omega)^{\mathbf{A}}V + \mathbf{G}_{\mathbf{A}} \tag{3} $$

where $\mathbf{M}_A \in \mathbb{R}^{6\times6}$ is the mass matrix, $\mathbf{C}_{\mathbf{A}}({}^{\mathbf{A}}\omega) \in \mathbb{R}^{6\times6}$ represents the Coriolis and centrifugal terms, ${}^{\mathbf{A}}F^{*} \in \mathbb{R}^6$ is the net force/moment vector, and $\mathbf{G}_{\mathbf{A}} \in \mathbb{R}^6$ is the gravity vector.

The linear parameterization expression for the required rigid body dynamics in a control design, can be written as

$$ \mathbf{Y}_{\mathbf{A}}\theta_{\mathbf{A}} \overset{\text{def}}{=} \mathbf{M}_{\mathbf{A}}\frac{d}{dt}({}^{\mathbf{A}}V_{\mathrm{r}}) + \mathbf{C}_{\mathbf{A}}({}^{\mathbf{A}}\omega)^{\mathbf{A}}V_{\mathrm{r}} + \mathbf{G}_{\mathbf{A}}. \tag{4} $$

In Eq. (4), the regressor matrix $\mathbf{Y}_A \in \mathbb{R}^{6\times13}$ and parameter vector $\theta_{\mathbf{A}} \in \mathbb{R}^{13}$ are specified in [21].

Finally, the required net force/moment vector for the *rigid links* can be presented as

$$ {}^{\mathbf{A}}F_r^{*} = \mathbf{Y}_{\mathbf{A}}\theta_{\mathbf{A}} + K_{\mathbf{A}}({}^{\mathbf{A}}V_r - {}^{\mathbf{A}}V) \tag{5} $$

where $K_{\mathbf{A}}$ denotes the velocity feedback control gain.

III. Kinematics and Dynamics Model for the HSEA

In SEA actuators, the spring is used to decouple the actuator from the environment. Typically, the HSEA consists of a hydraulic cylinder, which is connected in a series with a spring and a control servo-valve. The one degrees-of-freedom (DOF) prototype for an HSEA is illustrated in Fig. 1, where the spring stiffness is designed to be symmetric in both directions. One method to estimate a cylinder force is to use chamber pressures and cylinder areas. Normally, the cylinder chamber pressures provide inaccurate estimation for the cylinder force due to noise of the signals. In contrast, in the HSEA, with the known spring stiffness and spring compression, the spring can be used as a force sensor. The spring placement between the output power shaft and the load enables to sensing of external forces from the load side.

In this study, the main focus is to design a model-based controller for the HSEA using the VDC approach as a framework. This approach provides a dynamics subsystem model-based control design method for complex robot systems [22]. The current state-of-the-art control performance of heavy-duty hydraulic manipulators has been reached with the VDC approach, as reported in [17]. The HSEA in Fig. 1 has studied in heavy-duty applications with a load mass up to 200 kg.

The three main steps of the VDC approach are virtual decomposition of the entire system, coordinate frame attachment to subsystems, and simple oriented graph (SOG) presentation. In this section, the main steps are presented in detail and then the kinematics and dynamics modeling for the HSEA in Fig. 1 are given.

A. Virtual Decomposition of the HSEA

First, the entire system needs to be virtually decomposed into subsystems by placing conceptual *virtual cutting points* (VCPs) in the studied system. VCP comprose directed separation points the between successive subsystems for the six-dimensional force/moment relation to these subsystems. A

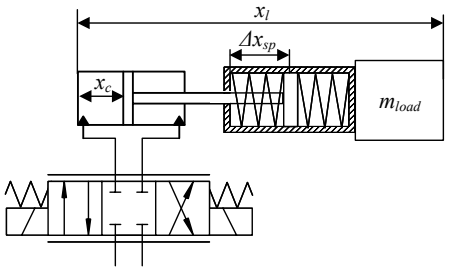

Fig. 1. Prototype for the HSEA

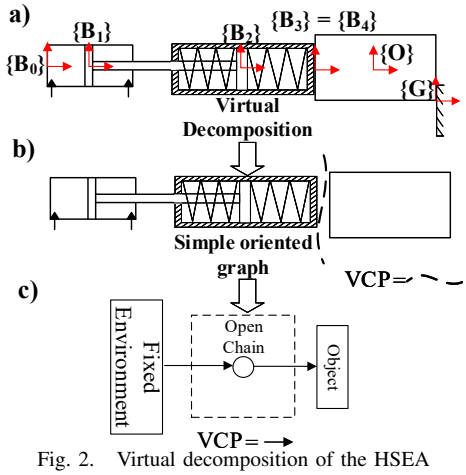

Fig. 2. Virtual decomposition of the HSEA

VCP is simultaneously interpreted driving for one subsystem and driven the VCP for another. The driven VCP is a point to which the force/moment vector is exerted, and the driving VCP is a point from which the force/moment vector is exerted. Virtual decomposition for the HSEA is expressed in Fig. 2b. As a results, the entire system can be modeled with two subsystem, which are called the *object* and *open chain*.

The dynamics between subsystems in a virtual decomposition system can be representing as an SOG [21]. The SOG represents the rigid links as nodes and the force/moment directions as directed edges. The SOG for the HSEA is given in Fig. 2c, where the subsystem of the hydraulic cylinder with a spring is represented by a dashed line.

The kinematic and dynamics of the subsystems can be modeled by allocating fixed coordinate frames to the subsystems. The used coordinate frames for the HSEA are presented in Fig. 2a. All coordinate frames in Fig. 2a are attached so that the z-axis point out from the paper. The frame $\mathbf{B}_0$ is fixed to cylinder base, $\mathbf{B}_1$ is fixed to cylinder piston, frame $\mathbf{B}_2$ is fixed to spring connecting point and $\mathbf{B}_3$ at the end of the cylinder. Frame $\mathbf{O}$ is fixed to load center of the mass and $\mathbf{G}$ at the end of the load.

B. Kinematics Equations for the HSEA

According to Eq. (1), the linear/angular velocity vectors in cylinder coordinate frames in Fig. 2a can be written as

$$ {}^{\mathbf{B}_1}V = {}^{\mathbf{B}_0}\mathbf{U}_{\mathbf{B}_1}^{T}\,{}^{\mathbf{B}_0}V + \mathbf{z}\dot{x}_c \tag{6} $$

$$ {}^{\mathbf{B}_2}V = {}^{\mathbf{B}_1}\mathbf{U}_{\mathbf{B}_2}^{T}\,{}^{\mathbf{B}_1}V \tag{7} $$

$$ {}^{\mathbf{B}_3}V = {}^{\mathbf{B}_0}\mathbf{U}_{\mathbf{B}_3}^{T}\,{}^{\mathbf{B}_0}V + \mathbf{z}\dot{x}_l \tag{8} $$

where $\mathbf{z} = [1\,0\,0\,0\,0\,0]^T$, $\dot{x}_c$ is the cylinder piston velocity, and $\dot{x}_l$ is the load velocity. In Eq. (6), the linear/angular velocity

vector ${}^{\mathbf{B}_0}V = [0\ 0\ 0\ 0\ 0\ 0]^T$ because in this paper, the base frame position is fixed. As Fig. 2 demonstrates, the cylinder is connected in a series with spring. Therefore, the cylinder velocity can be calculated as

$$\dot{x}_c = \dot{x}_l + \dot{x}_{sp} \tag{9}$$

where $\dot{x}_l$ is the measured load velocity and $\dot{x}_{sp}$ is the spring velocity.

C. Kinematics of the Load

The kinematic model for the load object can be defined according to Eq. (1) and Fig. 2a as

$${}^{\mathbf{O}}V = {}^{\mathbf{B}_4}\mathbf{U}_{\mathbf{O}}^{T\,\mathbf{B}_4}V = {}^{\mathbf{G}}\mathbf{U}_{\mathbf{O}}^{T\,\mathbf{G}}V. \tag{10}$$

Velocity vector ${}^{\mathbf{G}}V$ describes the velocity of the object.

D. Dynamics of the Load Object

The load object force/moment vector can be written according to Eq. (3) as

$${}^{\mathbf{O}}F^* = \mathbf{M}_{\mathbf{O}}\frac{d}{dt}({}^{\mathbf{O}}V) + \mathbf{C}_{\mathbf{O}}({}^{\mathbf{O}}\omega)^{\mathbf{O}}V + \mathbf{G}_{\mathbf{O}}. \tag{11}$$

On the other hand,

$${}^{\mathbf{O}}F^* = {}^{\mathbf{O}}\mathbf{U}_{\mathbf{B}_4}{}^{\mathbf{B}_4}F - {}^{\mathbf{O}}\mathbf{U}_{\mathbf{G}}{}^{\mathbf{G}}F \tag{12}$$

holds for the load object. Force vector ${}^{\mathbf{G}}F$ describes the external contact force between the object and environment.

E. Dynamics of the HSEA Open Chain

The dynamics relations for the HSEA *open chain* can be written, in view of Eq. 3, as

$$\begin{aligned}
{}^{\mathbf{B}_0}F^* &= \mathbf{M}_{\mathbf{B}_1}\frac{d}{dt}({}^{\mathbf{B}_1}V) + \mathbf{C}_{\mathbf{B}_1}({}^{\mathbf{B}_1}\omega)^{\mathbf{B}_1}V + \mathbf{G}_{\mathbf{B}_1} && (13)\\
{}^{\mathbf{B}_1}F^* &= \mathbf{M}_{\mathbf{B}_2}\frac{d}{dt}({}^{\mathbf{B}_2}V) + \mathbf{C}_{\mathbf{B}_2}({}^{\mathbf{B}_2}\omega)^{\mathbf{B}_2}V + \mathbf{G}_{\mathbf{B}_2} && (14)\\
{}^{\mathbf{B}_2}F^* &= \mathbf{M}_{\mathbf{B}_3}\frac{d}{dt}({}^{\mathbf{B}_3}V) + \mathbf{C}_{\mathbf{B}_3}({}^{\mathbf{B}_3}\omega)^{\mathbf{B}_3}V + \mathbf{G}_{\mathbf{B}_3}. && (15)
\end{aligned}$$

Therefore, the total force/moment vectors in coordinate frames can be written as

$$\begin{aligned}
{}^{\mathbf{B}_2}F &= {}^{\mathbf{B}_2}F^* + {}^{\mathbf{B}_2}\mathbf{U}_{\mathbf{B}_3}{}^{\mathbf{B}_3}F && (16)\\
{}^{\mathbf{B}_1}F &= {}^{\mathbf{B}_1}F^* + {}^{\mathbf{B}_1}\mathbf{U}_{\mathbf{B}_2}{}^{\mathbf{B}_2}F && (17)\\
{}^{\mathbf{B}_0}F &= {}^{\mathbf{B}_0}F^* + {}^{\mathbf{B}_0}\mathbf{U}_{\mathbf{B}_1}{}^{\mathbf{B}_1}F. && (18)
\end{aligned}$$

Now, the hydraulic cylinder force in coordinate frame $\mathbf{B}_1$ can be presented from Eq. (17) as

$$f_c = \mathbf{z}^{\mathbf{B}_1}F \tag{19}$$

where $\mathbf{z} = [1\ 0\ 0\ 0\ 0\ 0]$.

IV. Control Equations Design for the HSEA

Next, the control equations for the subsystems in Fig. 2b are presented. As Fig. 2 showed, the control system includes a hydraulic cylinder and a servo-valve. The control equations for the hydraulic servo-valve with fluid dynamics are specified closely in [18] and [21] with corresponding control equations. In view of the VDC approach, these modular equations can be incorporated into the control design when kinematics and dynamics equations are defined as in accordance with the approach. In the framework of the VDC, the format of required velocity includes the desired velocity and one or more terms, which are related to control errors. In the control design, control equations are designed by calculating required kinematics and dynamics equations in every coordinate frame in Fig. 2a.

A. Required Kinematics of the HSEA

The required linear/angular velocities for the HSEA *open chain* can be presented as follows, in view of Eqs. 6–8

$$\begin{aligned}
{}^{\mathbf{B}_1}V_r &= {}^{\mathbf{B}_0}\mathbf{U}_{\mathbf{B}_1}^{T\,\mathbf{B}_0}V_r + \mathbf{z}\dot{x}_{cr} && (20)\\
{}^{\mathbf{B}_2}V_r &= {}^{\mathbf{B}_1}\mathbf{U}_{\mathbf{B}_2}^{T\,\mathbf{B}_1}V_r && (21)\\
{}^{\mathbf{B}_3}V_r &= {}^{\mathbf{B}_0}\mathbf{U}_{\mathbf{B}_3}^{T\,\mathbf{B}_0}V_r + \mathbf{z}\dot{x}_{lr} && (22)
\end{aligned}$$

where $\mathbf{z} = [1\ 0\ 0\ 0\ 0\ 0]^T$, $\dot{x}_{lr}$ is the load velocity, and $\dot{x}_{cr}$ is the required cylinder piston velocity.

B. Required Kinematics of the Load

The load object's required kinematics can be specified, considering Eq. (10), as

$${}^{\mathbf{O}}V_r = {}^{\mathbf{B}_4}\mathbf{U}_{\mathbf{O}}^{T\,\mathbf{B}_4}V_r = {}^{\mathbf{G}}\mathbf{U}_{\mathbf{O}}^{T\,\mathbf{G}}V_r. \tag{23}$$

The velocity vector ${}^{\mathbf{G}}V_r$ describes the required velocity of the object.

C. Required Dynamics of the Load Object

The required net force/moment vector of the load object can be written, by reusing Eq. (5), as

$${}^{\mathbf{O}}F_r^* = \mathbf{Y}_{\mathbf{O}}\theta_{\mathbf{O}} + \mathbf{K}_{\mathbf{O}}({}^{\mathbf{O}}V_r - {}^{\mathbf{O}}V). \tag{24}$$

So, by using Eq. (12), the net force/moment vector in frame $\{\mathbf{B}_4\}$ can be presented as

$${}^{\mathbf{B}_4}F_r^* = {}^{\mathbf{B}_4}\mathbf{U}_{\mathbf{O}}{}^{\mathbf{B}_4}F_r - {}^{\mathbf{B}_4}\mathbf{U}_{\mathbf{G}}{}^{\mathbf{G}}F_r. \tag{25}$$

The force vector ${}^{\mathbf{G}}F_r$ describes the required external force vector between object and environment.

D. Required Dynamics of the HSEA

According to the required kinematics model for the HSEA *open chain* in Eqs. (20)–(22) and according Eq. (5), the required net force/moment vectors for rigid links can be defined as

$$\begin{aligned}
{}^{\mathbf{B}_0}F_r^* &= \mathbf{Y}_{\mathbf{B}_0}\theta_{\mathbf{B}_0} + \mathbf{K}_{\mathbf{B}_0}({}^{\mathbf{B}_0}V_r - {}^{\mathbf{B}_0}V) && (26)\\
{}^{\mathbf{B}_1}F_r^* &= \mathbf{Y}_{\mathbf{B}_1}\theta_{\mathbf{B}_1} + \mathbf{K}_{\mathbf{B}_1}({}^{\mathbf{B}_1}V_r - {}^{\mathbf{B}_1}V) && (27)\\
{}^{\mathbf{B}_2}F_r^* &= \mathbf{Y}_{\mathbf{B}_2}\theta_{\mathbf{B}_2} + \mathbf{K}_{\mathbf{B}_2}({}^{\mathbf{B}_2}V_r - {}^{\mathbf{B}_2}V). && (28)
\end{aligned}$$

Then, it follows from Eqs. (5), (26), and (28) that the force/moment vectors for the HSEA *open chain* can be defined as

$$
\begin{aligned}
{}^{\mathbf{B}_2}F_r &= {}^{\mathbf{B}_2}F_r^* + {}^{\mathbf{B}_2}\mathbf{U}_{\mathbf{B}_3}{}^{\mathbf{B}_3}F_r && (29)\\
{}^{\mathbf{B}_1}F_r &= {}^{\mathbf{B}_1}F_r^* + {}^{\mathbf{B}_1}\mathbf{U}_{\mathbf{B}_2}{}^{\mathbf{B}_2}F_r && (30)\\
{}^{\mathbf{B}_0}F_r &= {}^{\mathbf{B}_0}F_r^* + {}^{\mathbf{B}_0}\mathbf{U}_{\mathbf{B}_1}{}^{\mathbf{B}_1}F_r. && (31)
\end{aligned}
$$

Finally, the required linear cylinder force can be calculated from Eq. (30)

$$f_{cr} = \mathbf{z}^{\mathbf{B}_1}F_r \tag{32}$$

where $\mathbf{z}$ = [1 0 0 0 0 0].

V. Impedance Controller for the HSEA

HSEA actuators provide a high power-to-weight ratio compared to electric SEAs. Therefore, HSEAs are suitable for moving heavy loads in many industrial tasks. Interactions between the environment and manipulator with a high contact force may stress mechanical structure. For this reason, the impedance control designs for HSEAs have been an active research subject over the past decade. A novel impedance control method in a Cartesian space for heavy-duty hydraulic manipulators the framework of the VDC approach is presented in [23]. In this study, the impedance control method is incorporated in the control design.

Fig. 1 shows that the HSEA consists of a spring, which is connected in the series with a hydraulic spring. By connecting two elastic springs in a series, the effective stiffness of the system is reduced. In this study, the selected spring stiffness is illustrated in Fig. 3. As Fig. 3 shows, the spring stiffness is not linear due to pretension of the spring. The selection of the spring is presented with more details in [24]. The contact force of the HSEA can be estimated by using spring stiffness and measured spring compression. Therefore, the contact force can be calculated as

$$
\begin{aligned}
f_e = {} & \eta(x_{sp})(\eta(x_{pr-x_{sp}})\eta(x_{sp})k_1x_{sp}+\\
& \eta(x_{sp}-x_{pr})k_2+2k_1) - \eta((-x_{sp})(\eta(x_{pr}+x_{sp})\\
& \eta(-x_{sp})k_1(-x_{sp}) + \eta(-x_{sp}-x_pr)k_2+2k_1) \qquad (33)
\end{aligned}
$$

where k_1 and k_2 are the slope gains for the spring stiffness, x_{pr} is a pretension area, x_{sp} is the spring compression, and f_e is a contact force. The switching function is

$$\eta(x) = \frac{\tanh([x-x_o]/c_\eta)+1}{2} \tag{34}$$

where x_o is a sufficiently small offset constant parameter, and c_η is a sufficiently small constant.

Now, the control law for a target impedance can be presented, in view of [25], as

$$f_d - f_e = M_d(\ddot{x}_l - \ddot{x}_{ld}) + K_d(\dot{x}_l - \dot{x}_{dl}) + K_x(x_l - x_{dl}) \tag{35}$$

where M_d is inertia gain, K_d is the damping gain, and K_x is the stiffness gain of the target impedance. In this study, the dynamics parameters M_d, K_d and K_x are scalars because only 1-DOF contact force is studied. In Eq. (35), x_l, $\dot{x}_l$ and $\ddot{x}_l$ represent the measured position, velocity, and acceleration

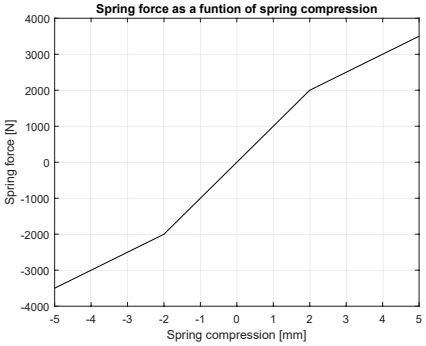

Fig. 3. Spring force as a function of spring compression

of the load, and x_{dl}, $\dot{x}_{dl}$ and $\ddot{x}_{dl}$ are the desired values respectively. In Eq. (35) the desired force is selected to be $f_d = 0$. The dynamics of the environment can be modeled as pure damping and stiffness to make the model manageable for the control. Now, the impedance control law can be rewritten as

$$f_d - f_e = K_d(\dot{x}_l - \dot{x}_{dl}) + K_x(x_l - x_{dl}). \tag{36}$$

As specified in [23], by assuming that a stiffness and a damping gain are selected so that their magnitudes are not subject to unstable behavior and that desired target impedance is attainable, the impedance control law in Eq. (36) can be rewritten as

$$\dot{x}_r = \dot{x}_{dl} + D_x(x_{dl} - x_l) + D_d(f_d - f_e) \tag{37}$$

where $\dot{x}_r$ is a required velocity, D_x is a stiffness gain, and D_d is a damping gain. The required velocity $\dot{x}_r$ is a unique property of the VDC approach, which generally consists of a desired velocity and control error related terms. The required velocity serves as a reference trajectory to the system. In Eq. (37), the D_x and D_d are scalar gains, which are defined as

$$
\begin{aligned}
D_d &= K_d^{-1} && (38)\\
D_x &= K_xK_d^{-1}. && (39)
\end{aligned}
$$

The impedance control law in Eq. (37) is equal to Eq. (36) only if gains D_x and D_d are defined as in Eqs. (38)–(39) more detail in [26]. As Eq. (37) shows, this impedance control method provides a parallel force and position control.

Now, velocity vectors in Eq. (10) and Eq. (23) and force vectors in Eq. (12) and Eq. (25) in coordinate frame $\mathbf{G}$ (see Fig. 2a) can be defined as

$$
\begin{aligned}
{}^{\mathbf{G}}V = \mathbf{z}\dot{x}_l \quad {}^{\mathbf{G}}V_r = \mathbf{z}\dot{x}_r && (40)\\
{}^{\mathbf{G}}F = \mathbf{z}f_e \quad {}^{\mathbf{G}}F_r = \mathbf{z}f_r. && (41)
\end{aligned}
$$

where $\mathbf{z}$ = $[1\ 0\ 0\ 0\ 0\ 0]^T$.

VI. Experimental Results

In this section, the control of the proposed controller was verified with a 1-DOF full-scale experimental setup, which is presented in Fig. 4. In the setup, the real-time control interface was implemented with a Beckhoff CX2030 controller with a sampling rate of 1000 Hz. The size of the hydraulic cylinder was ϕ32/18-400. The cylinder was

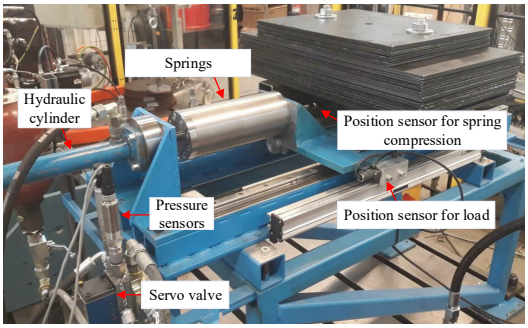

Fig. 4. 1-DOF HSEA experimental setup

controlled by using an NG6 size servo solenoid valve with a nominal flow rate of 40 l/min at 3.5 MPa per control notch. The cylinder chamber pressures were measured with UNIK 5000 pressure transmitters with a measuring range of 25 MPa. The supply pressure of the setup was set to 20 MPa. The spring compression was measured using an MTS linear position sensor with a measurement range of 0.015 m and load position was measured with a Heidenhein linear position sensor with a measurement range of a 0.54 m. The used load mass was 200 kg. The used spring stiffness (see. Fig.3) was 1000 N/mm in pretension area and 500 N/mm after that.

In both experiments, the proposed controller was tested by using a point-to-point quintic reference trajectory designed for the load position. The damping and the stiffness gains of the impedance control (see Eq. (37)) were set as a compromise between a system damping and a settling time. In the experiments, gains in Eq. (38) and Eq. (39) was set to $D_x = 5 \times 10^{-5}$ and $D_d = 1.75$.

In the first experiment, the load was driven to contact with a stiff environment. The load position during the contact motion is presented in Fig. 5. The contact point in Fig. 5 was set to 0.496 m, which was reached 4 s. As Fig. 5 shows, the proposed controller efficiently limits the load position in a contact motion. The load position errors without contact are about 1.4 mm and 1.8 mm for the positive and negative directions, respectively. Contact with the environment caused a peak for the position error, and the static error during contact was 1.5 mm. The static error contact force results from a parallel force and position control. Fig. 6, the cylinder position during the contact motion is presented. As Fig. 6 demonstrates, the maximum position error of the hydraulic cylinder for position direction is about 1.2 mm , and for the negative direction it is about 1.6 mm.

As Eq. (37) shows, in the case of the proposed impedance controller, the contact force is included to load the velocity reference with a position error term. In Fig. 7, the contact force effects to the load velocity reference are presented. As Fig. 7 shows, the contact at time 4 s efficiently drops the load reference velocity when the contact force and position error start to rise.

In both experiments, the contact force was estimated using Eq. (33). Fig. 8 demonstrates, the contact force with and without the proposed impedance controller. As Fig. 8 shows, the proposed impedance controller significantly decreases the actuator's contact force with the environment.

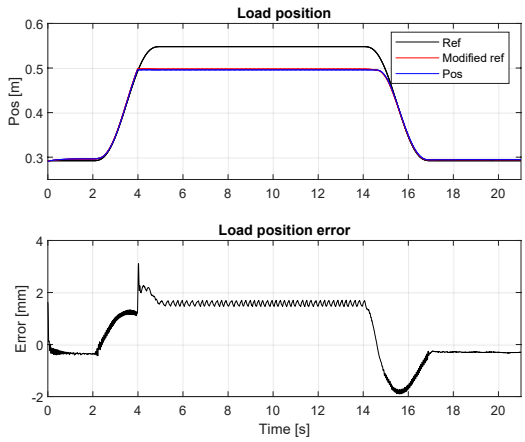

Fig. 5. Load position during the contact motion with stiff environment

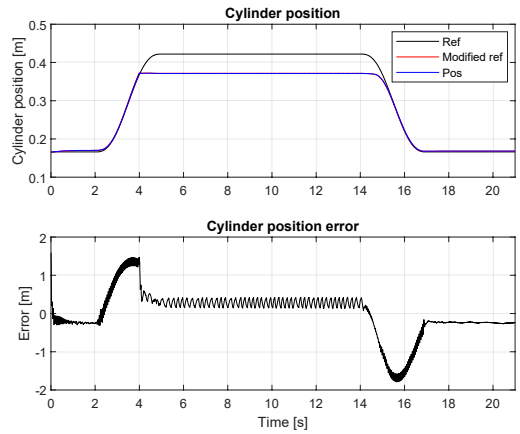

Fig. 6. Cylinder position during the contact motion with stiff environment

In the second experiment, the load was put into contact with a soft environment. The load position during the contact motion is presented in Fig. 9. The contact point in Fig. 9 was set to 0.466 m, which was reached at time 3.8 s. Compared to Fig. 5, which represents a stiff environment, in Fig. 9 with the soft environment the static error is a litter higher. Still, the proposed controller can be limited efficiently by the load position during the contact motion.

The experimental results verifies that proposed impedance control method can efficiently damps the contact between the HSEA system and stiff and soft environment.

VII. Conclusions

This paper focused on proposing a model-based controller design for HSEAs. The target impedance control for an HSEA is also presented by incorporating the proposed controller as an inner-loop controller with a previously designed impedance control method. Experimental results with a real-size 1-DOF experimental setup verified that the proposed controller can efficiently control the contact force between the actuator and the environment. In future research, the proposed controller will be studied in a real world multi-DOF hydraulic manipulator.

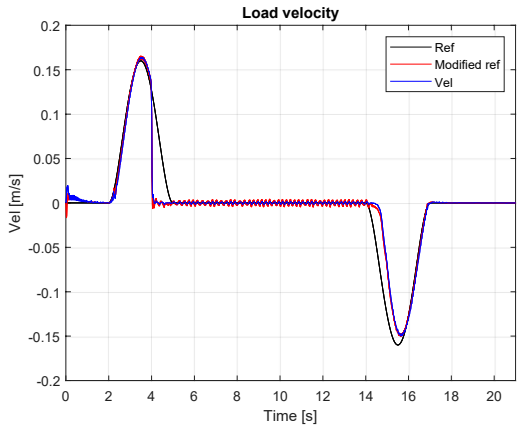

Fig. 7. Load velocity during the contact motion with stiff environment

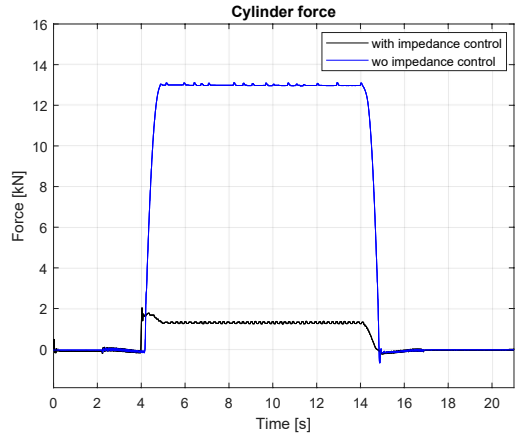

Fig. 8. Cylinder force with and without impedance control

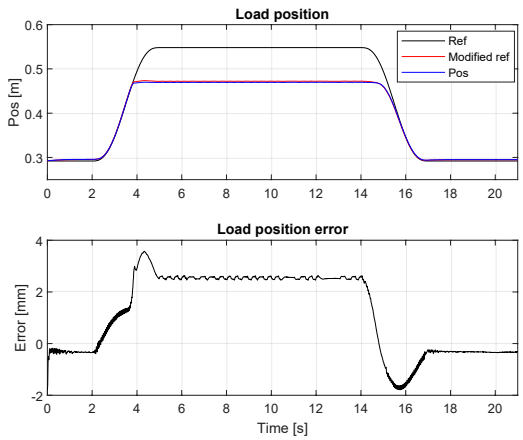

Fig. 9. Load position during the contact motion with soft environment

REFERENCES

[1] A. Albu-Schäffer, C. Ott, and G. Hirzinger, "A unified passivity-based control framework for position, torque and impedance control of flexible joint robots," *The international journal of robotics research*, vol. 26, no. 1, pp. 23–39, 2007.

[2] C. Loughlin, A. Albu-Schäffer, S. Haddadin, C. Ott, A. Stemmer, T. Wimböck, and G. Hirzinger, "The dlr lightweight robot: design and control concepts for robots in human environments," *Industrial Robot: an international journal*, 2007.

[3] A. Albu-Schaffer, C. Ott, U. Frese, and G. Hirzinger, "Cartesian impedance control of redundant robots: Recent results with the dlr-light-weight-arms," in *International Conference on Robotics and Automation*, vol. 3. IEEE, 2003, pp. 3704–3709.

[4] C. Lee, S. Kwak, J. Kwak, and S. Oh, "Generalization of series elastic actuator configurations and dynamic behavior comparison," in *Actuators*, vol. 6, no. 3. Multidisciplinary Digital Publishing Institute, 2017, p. 26.

[5] B. Lee, C. Knabe, V. Orekhov, and D. Hong, "Design of a human-like range of motion hip joint for humanoid robots," in *International Design Engineering Technical Conferences and Computers and Information in Engineering Conference*. ASME, 2014.

[6] W. Takano, H. Kanayama, T. Takahashi, T. Moridaira, and Y. Nakamura, "A data-driven approach to probabilistic impedance control for humanoid robots," *Robotics and Autonomous Systems*, vol. 124, p. 103353, 2020.

[7] D. W. Robinson, J. E. Pratt, D. J. Paluska, and G. A. Pratt, "Series elastic actuator development for a biomimetic walking robot," in *International Conference on Advanced Intelligent Mechatronics*. IEEE, 1999, pp. 561–568.

[8] J. Pratt, B. Krupp, and C. Morse, "Series elastic actuators for high fidelity force control," *Ind. Robot: An International Journal*, 2002.

[9] J. E. Pratt and B. T. Krupp, "Series elastic actuators for legged robots," in *Unmanned Ground Vehicle Technology Vi*, vol. 5422. International Society for Optics and Photonics, 2004, pp. 135–144.

[10] S. Oh and K. Kong, "High-precision robust force control of a series elastic actuator," *IEEE/ASME Trans. on Mechatronics*, vol. 22, no. 1, pp. 71–80, 2016.

[11] Y. Zhao, N. Paine, S. J. Jorgensen, and L. Sentis, "Impedance control and performance measure of series elastic actuators," *IEEE Trans. on Industrial Electronics*, vol. 65, no. 3, pp. 2817–2827, 2017.

[12] A. Calanca and P. Fiorini, "Understanding environment-adaptive force control of series elastic actuators," *IEEE/ASME Trans. on Mechatronics*, vol. 23, no. 1, pp. 413–423, 2018.

[13] D. W. Robinson and G. A. Pratt, "Force controllable hydro-elastic actuator," in *Proceedings 2000 ICRA. Millennium Conference. IEEE International Conference on Robotics and Automation.*, vol. 2. IEEE, 2000, pp. 1321–1327.

[14] A. Flores-Abad, M. Nandayapa, and M. A. Garcia-Teran, "Force sensorless impedance control for a space robot to capture a satellite for on-orbit servicing," in *Aerospace Conference*.

[15] N. Paine, S. Oh, and L. Sentis, "Design and control considerations for high-performance series elastic actuators," *IEEE/ASME Trans. on Mechatronics*, vol. 19, no. 3, pp. 1080–1091, 2013.

[16] K.-x. Ba, G.-l. Ma, B. Yu, Z.-g. Jin, Z.-p. Huang, J.-x. Zhang, and X.-d. Kong, "A nonlinear model-based variable impedance parameters control for position-based impedance control system of hydraulic drive unit," *Int. Journal of Control, Automation and Systems*, pp. 1–12.

[17] J. Mattila, J. Koivumäki, D. G. Caldwell, and C. Semini, "A survey on control of hydraulic robotic manipulators with projection to future trends," *IEEE/ASME Trans. on Mech.*, vol. 22, no. 2, pp. 669–680, 2017.

[18] J. Koivumäki and J. Mattila, "Stability-guaranteed force-sensorless contact force/motion control of heavy-duty hydraulic manipulators," *IEEE Trans. Robotics*, vol. 31, no. 4, pp. 918–935, 2015.

[19] ——, "Stability-guaranteed impedance control of hydraulic robotic manipulators," *IEEE/ASME Trans. on Mechatronics*, vol. 22, no. 2, pp. 601–612, 2017.

[20] J. Koivumäki, W.-H. Zhu, and J. Mattila, "Energy-efficient and high-precision control of hydraulic robots," *Control Engineering Practice*, vol. 85, pp. 176–193, 2019.

[21] W.-H. Zhu, *Virtual decomposition control: toward hyper degrees of freedom robots*. Springer Science & Business Media, 2010, vol. 60.

[22] W.-H. Zhu, Y.-G. Xi, Z.-J. Zhang, Z. Bien, and J. De Schutter, "Virtual decomposition based control for generalized high dimensional robotic systems with complicated structure," *IEEE Trans. Robot. Autom.*, vol. 13, no. 3, pp. 411–436, 1997.

[23] J. Koivumäki and J. Mattila, "Stability-guaranteed impedance control of hydraulic robotic manipulators," *IEEE/ASME Trans. Mechatronics*, vol. 22, no. 2, pp. 601–612, 2017.

[24] X. Cao, M. M. Aref, and J. Mattila, "Design and control of a flexible joint as a hydraulic series elastic actuator for manipulator application," 2019, [Accepted].

[25] H. Neville, "Impedance control: An approach to manipulation: Part i–iii," *Trans. of ASME Journal of Dynamic System, Measurement, and Control*, vol. 107, p. 1, 1985.

[26] J. Koivumäki and J. Mattila, "Adaptive and nonlinear control of discharge pressure for variable displacement axial piston pumps," *ASME J. Dyn. Syst., Meas., Control*, vol. 139, no. 10, 2017.